Available online at www.sciencedirect.com
SCIENCE DIRECT®
ELSEVIER
Nuclear Physics A 752 (2005) 633c–644c
NUCLEAR PHYSICS A

# Laser Induced Nuclear Physics and Applications

K.W.D. Ledingham,

Department of Physics, University of Strathclyde, Glasgow, G4 0NG, Scotland, and AWE plc, Aldermaston, Reading,RG7 4PR,UK

## Preamble

Laser induced beams of protons, neutrons and gamma rays using short pulse lasers is currently important principally because of the potential applications e.g. isotope production, transmutation studies, laser induced fission, heavy ion fusion reactions, neutron production and radiography, fast ignitor and spallation studies of neutrons. Although the Strathclyde group in collaboration with teams from Imperial College and the Rutherford Appleton Laboratory have been at the forefront of many of these applications this presentation only deals with laser induced PET isotope production and laser transmutation studies. These two applications will be dealt with in separate sections.

## 1. PET isotope production

### Introduction

Recent experiments have demonstrated that laser-solid interactions at intensities greater than $10^{19}$Wcm$^{-2}$ can produce fast electron beams of several hundred MeV [1], several MeV $\gamma$ rays, up to 58 MeV proton beams [2], and heavier ions [3] of up to 7 MeV/nucleon. One of the exciting applications of the high energy proton beams is the production of radioactive isotopes for Positron Emission Tomography (PET). PET is a form of medical imaging requiring the production of short lived positron emitting isotopes $^{11}$C, $^{13}$N, $^{15}$O and $^{18}$F, by proton irradiation of natural/enriched targets using cyclotrons. PET development has been hampered due to the size and shielding requirements of the nuclear installations but recent results, have shown when an intense laser beam interacts with solid targets, tens of MeV protons capable of producing PET isotopes are generated [4-6]

## 2. Positron Emission Tomography

0375-9474/$ – see front matter 
doi:10.1016/j.nuclphysa.2005.02.132

Positron Emission Tomography (PET) is a powerful medical diagnostic/imaging technique requiring the production of short-lived (2 min – 2 hour) positron emitting isotopes. The PET process involves the patient receiving an injection of a pharmaceutical labeled with a short-lived β+ emitting source which collects in 'active' areas of the body such as tumours. The principal tracers used in the PET technique are $^{11}C$, $^{13}N$, $^{15}O$ and $^{18}F$. Many chemical compounds can be labeled with positron emitting isotopes and their bio-distribution can be determined by PET imaging as a function of time. However the most commonly used radiopharmaceutical is 2-fluoro-2-deoxyglucose 2-[$^{18}$F]FDG. Over the last few years the value of PET FDG in the management of cancer patients has been widely demonstrated. Figure 1 highlights the success rate of PET in diagnosing lung cancer compared with conventional x-ray computed tomography (CT) scanning.

PET isotopes are generally produced using energetic proton beams produced by cyclotrons or van de Graafs via (p,n) or (p,α) reactions using methods completely understood by this conference. Proton induced reactions are favoured since the resultant isotope differs in atomic number from the reactant, thus simplifying the separation process and makes it possible to produce carrier free sources allowing the patient to be injected with the minimum amount of foreign material.

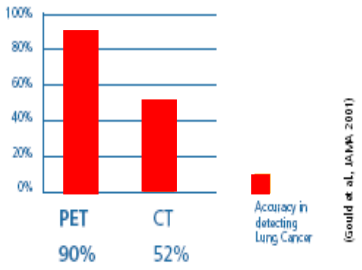


**Fig. 1.** Accuracy of PET in detecting lung cancer compared with x-ray CT scanning.

One of the main factors limiting the wider use of FDG PET imaging is the requirement for expensive infrastructure at the heart of which lies the cyclotron and the associated extensive radiation shielding. A more simplified approach to isotope production would be to develop a miniaturised, on site resource with eventual capability similar to that of a cyclotron. As was stated previously, recent results show when an intense laser beam ($I > 10^{19}$ W/cm$^2$) interacts with solid targets, beams of MeV protons capable of producing PET isotopes are generated. Recent reports have concentrated on some preliminary work carried out by this group [4,5] and Fritzler et al [6] on the production of PET isotopes using a high power laser . It should be pointed out at this stage that the laser approach is not intended to be a competitor of cyclotron sources but in the fullness of time as the lasers develop and become smaller this could be a complimentary approach.

As early as the seventies, it was proposed [7] that laser-driven electron acceleration was possible using intense laser light to produce a wake of oscillations in a plasma. Recently, 200 MeV electrons were measured using a compact high repetition rate laser [1]. Laser-plasma based accelerators have the potential to deliver accelerating gradients more than 1000 times higher than conventional accelerator technology, and on a compact scale.

## Proton Production with a High Intensity Laser

Recent advances in laser technology with the introduction of 'chirped pulse amplification [8] (CPA) have led to the development of multi-terawatt pulsed laser systems in many laboratories worldwide. After amplification, these laser pulses are recompressed to deliver $10^{18\text{-}20}$Wcm$^{-2}$ on target. Proposed techniques, including optical parametric chirped pulse amplification (OPCPA) [9,10] promise to extend the boundaries of laser science into the future and also reduce the large lasers used presently to compact table-top varieties.

High intensity laser radiation may now be applied in many traditional areas of nuclear science. As the laser intensity and associated electric field is increased then the electron quiver energy, the energy a free electron has in the laser field, increases dramatically. Thus, when laser radiation is focused onto solid and gaseous targets at intensities > $10^{18}$ Wcm$^{-2}$, electrons quiver with energies greater than their rest mass (0.511 MeV) creating relativistic plasmas [11]. At these intensities, the Lorentz force –e($v$ x **B**) due to the laser interacting with charged particles produces a pondermotive force allowing electrons to be accelerated into the target in the direction of laser propagation. The resulting electron energy distribution can be described by a quasi-Maxwellian distribution yielding temperatures (kT) of a few MeV [12].

The protons emanate from water and from hydrocarbons as contaminant layers on the surfaces of the solid targets. These contamination layers are due to the poor vacuum (~ $10^{-5}$ Torr) achievable in the target chambers The main mechanism thought to be responsible for proton acceleration is the production of electrostatic fields due to the separation of the electrons from the plasma ions. Proton beams are observed both in front of (blow-off direction) and behind (straight through direction) the primary target. In front of the target, ion beams are observed from the expansion of the plasma generated on the target surface, produced either by a prepulse or the rising edge of the main pulse itself, also known as “blow-off” plasma, directed normal to the target surface.

Several acceleration mechanisms have been proposed to describe where the protons in the straight through direction originate, either the front surface, back surface or both. One such mechanism is the Target Normal Sheath Acceleration (TNSA) [13]. In this scheme, shown in figure 2, the ion acceleration mechanism results from the cloud of hot electrons (generated in the blow-off plasma from the

laser pre-pulse interacting with the front surface of the target) traveling through the target and field ionizing the contaminant proton layer on the back surface of the target. The protons are then pulled off the back surface by the cloud of electrons and accelerated normal to the target to tens of MeV's in tens of μm. The initial laser pre-pulse may be of the order of $10^{-6}$ ( I ~ $10^{12\text{-}14}$ W/cm$^2$) of the main laser pulse, sufficient to ionize the front surface of the target. Thus, at the back of the target where no pre-plasma is formed, the accelerating field is greater, resulting in higher energy ions. Recent studies have reported on direct experimental evidence of back-surface ion acceleration form laser irradiated foils by using sputtering techniques to remove contaminants from both the front and back surfaces [14]. It has also been proposed that the protons are accelerated via an electrostatic sheath formed on the front surface of the target and dragged through the target to produce a proton beam at the rear of the target [15] Comparative reports on the ion acceleration schemes can be found in references [16,17].

Proton energies with an exponential distribution up to 58 MeV have been observed [2] for a laser pulse intensity of $3x10^{20}$ Wcm$^{-2}$ and production of greater than $10^{13}$ protons per pulse has been reported [18]. With the VULCAN laser at the RAL delivering close to petawatt powers, it is now possible to demonstrate the potential for high power lasers to produce intense radioactive sources.

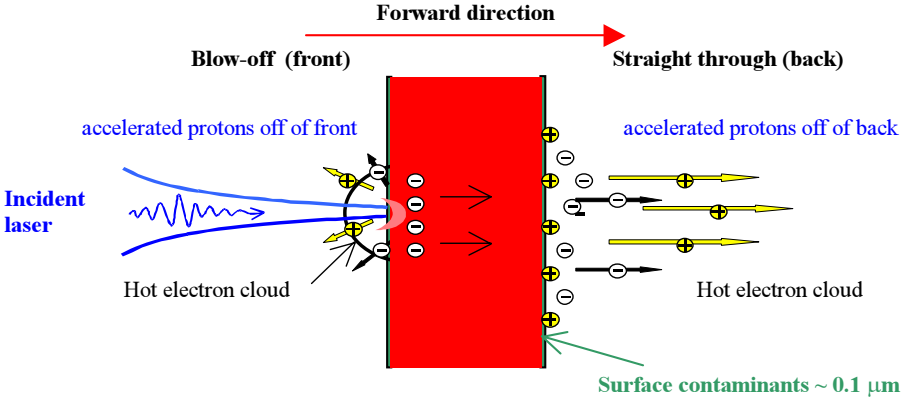


**Fig. 2.** Pictorial representation of the Target Normal Sheath Acceleration (TNSA) [13] scheme.

The new petawatt arm of the VULCAN Nd:Glass laser at RAL is employed in this experimental study. The 60 cm beam is focused to ~ 5.5 μm diameter spot using a 1.8 m focal length off-axis parabolic mirror, in a vacuum chamber evacuated to ~$10^{-4}$ mbar. The energy on target is between 220 and 300 J while the average pulse duration is 750 fs. The peak intensity is of the order of 2 x $10^{20}$ Wcm$^{-2}$.

### *Proton energy measurements*

To measure the energy spectra of the accelerated protons, nuclear activation techniques are employed. Copper stacks (5cm x 5cm) are positioned along the target normal direction and exposed to the protons accelerated from both the front and back surfaces of the primary target foil. Figure 3 shows an image of the experimental set up inside the chamber.

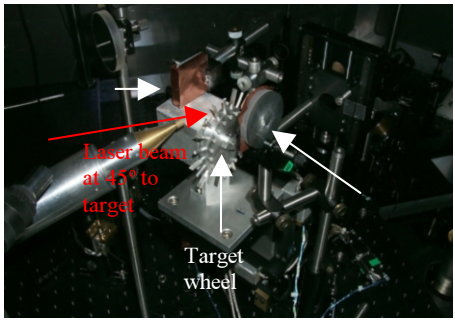


**Fig. 3.** Image of inside the target chamber showing the incident laser beam directed onto varying thicknesses of materials of foils held in a target wheel. The Copper stacks for proton energy measurements and Boron samples for $^{11}C$ production are shown.

The activity in the copper foils from the $^{63}Cu(p,n)^{63}Zn$ reaction with a half-life of 38 minutes is measured in a 3"x3" NaI coincidence system. The efficiency of the system is measured using a calibrated $^{22}Na$ source, thus the absolute activity can be determined. The measured activity in the foils from the $^{63}Cu(p,n)^{63}Zn$, convoluted with the reaction cross-section (shown in figure 4 (a)) and proton stopping powers is used to produce the energy distributions shown in figure 4 (b).

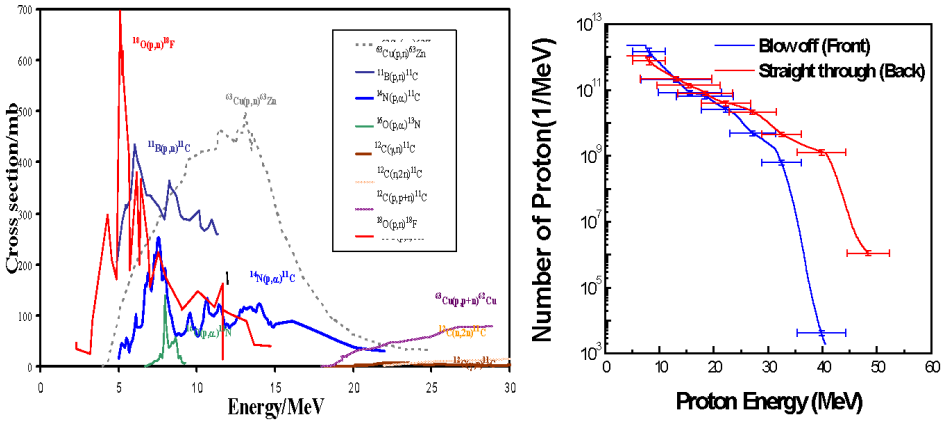


**Fig. 4.** (a) Experimentally measured cross-sections [19] for the nuclear reactions used to diagnose the proton spectra. Also shown are the cross-sections for the nuclear reactions described for the production of PET isotopes. (b) Typical proton spectra in front of and behind a 10 μ Al target. The number of protons generated per laser shot at about 300J and $2x10^{20}W/cm^2$ is typically $10^{12}$.

### *$^{18}F$ and $^{11}C$ generation*

The isotope $^{18}F$ is generated from a (p,n) reaction on $^{18}O$ enriched (96.5%) target. The enriched $^{18}O$ targets were irradiated in the form of 1.5mL of [$^{18}O$]$H_2O$ placed in a 20 mm diameter stainless steel target holder. For the production of $^{11}C$, the copper stacks described above were replaced by boron samples (5cm diameter and 3 mm thick). After irradiation, the boron targets were removed from the vacuum chamber and the $^{11}C$ activity produced by the (p,n) reaction on $^{11}B$ was measured in the coincidence system up to two hours after the laser shot, a safety precaution because of the high activity. The counting rate was determined at time zero and converted to Bq using a calibrated $^{22}Na$ source.

### *Target selection*

In order to determine the thickness of primary target which generated the highest activity sources, the $^{11}C$ activity generated in the secondary $^{11}B$ targets is measured as a function of sample material and thickness. The ratio of the back to front activities is shown in figure 5. This was carried out using the production of the PET isotope $^{11}C$ rather than the more novel $^{18}F$ because of the expensive cost of carrying out systematic work using the very expensive separated $^{18}O$ isotope as a target is prohibitive. It is clear from figure 5 that very thin targets provide the highest activity sources when the total activity produced per laser shot is the sum of the back and front activities.

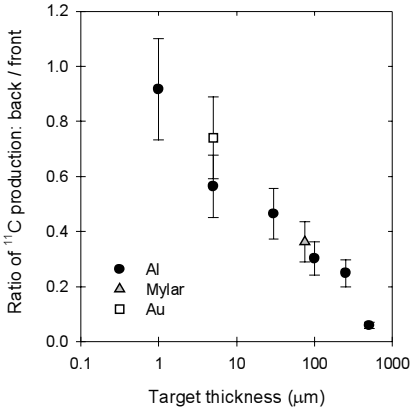


**Fig. 5.** Back/front ratio of $^{11}$C from the (p,n) reactions on $^{11}$B as a function of target thickness. At the highest pulse energy on target ~300J the $^{11}$C activity maximally was about $6x10^6$ Bq per shot on each side. This is greater than $10^7$Bq in total.

## *$^{18}$F and $^{11}$C production*

It was reported earlier that $^{18}$F is the most widely used tracer in clinical PET today due to its longer half-life allowing for the synthesis of a number of samples within a half-life decay of the isotope and because fluorine chemistry is readily introduced in many organic and bioinorganic compounds. It was necessary to determine how much $^{18}$F could be produced per laser shot. The isotope is generated from a (p,n) reaction on $^{18}$O enriched (96.5%) target. At the highest laser pulse energies (300J), $10^5$Bq total activity of $^{18}$F was produced (shown later).

The half-life for the $^{18}$F source is shown in figure 6. The measured half-life of 110± 3 mins was determined over more than three half-lifes and demonstrates the purity of the $^{18}$F source and agrees closely with the generally accepted value (109 mins). Also shown is the measured half-life of $^{11}$C of 20 minutes and agrees well with the accepted value.

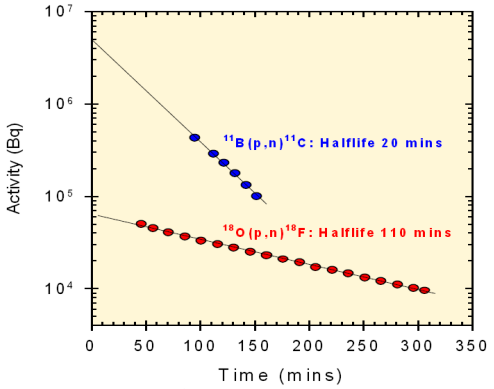


**Fig. 6.** The measured half-lifes for $^{18}$F and $^{11}$C. The values are close to the accepted ones indicating the purity of the sources produced.

Figure 7 summarises our measurements to date in this programme of research into laser-driven $^{11}$C and $^{18}$F PET isotope production on VULCAN. The red points [$^{11}$C] correspond to a number of different laser irradiances and pulse energies up to 300J with a pulse duration of ~ 750fs. The single blue triangular point is the activity from the $^{18}$F measurements at the highest laser pulse energy. The hatched areas at the top of the graph provide an indication for the level of required $^{18}$F activity (1GBq) from which an $^{18}$F-FDG patient dose would be generated and the required $^{11}$C activity (0.5 GBq), e.g. in the form of [$^{11}$C]CO.

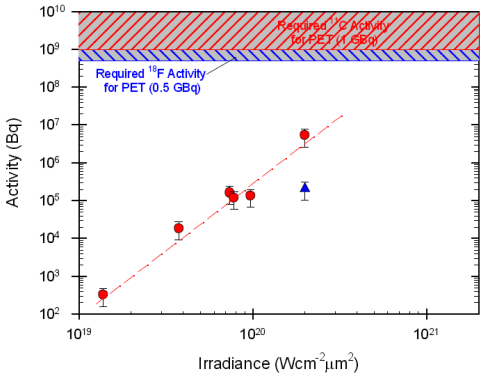


**Fig. 7.** The total activity (front and back) generated by a single laser shot for both $^{11}$C and $^{18}$F as a function of laser irradiance with pulse energies from 15 to 300J. The circles refer to $^{11}$C production and the single triangular point for $^{18}$F was measured at the highest energies.

## Future Developments and Conclusions

### *How to increase the PET isotope activity to $10^9$ Bq.*

. Although, the results presented here were obtained from a large single shot laser, it is important to highlight the progress made using compact high repetition rate lasers. Fritzler *et al* [6] have calculated that 13MBq of $^{11}$C can be generated using the LOA "table-top" laser (1J, 40fs) $6x10^{19}Wcm^{-2}$ after 30 minutes at 10Hz and that this can be extended to GBq using similar lasers with kHz repetition rates. Alternatively at JanUSP (Livermore) using a single pulse (8.5J, 100fs, 800nm) at $2x10^{20}Wcm^{-2}$, 4.4kBq of $^{11}$C was generated from a single laser shot [20]. Using a compact laser with similar specifications at 100 Hz after 30 minutes this would amount to close to GBq. A compact "table-top" laser system has recently been designed by Collier and Ross [21] for this purpose. In addition, the small scale POLARIS [22] all diode pumped petawatt laser currently being built at the Friedrich-Schiller University of Jena has the potential to deliver $10^{21}$ W/cm$^2$ ($\tau$ = 150 fs, E = 150 J, $\lambda \sim 1$ $\mu$m) with a repetition rate of 0.1 Hz.

## 2. Laser Induced Transmutation studies

One of the major problems of the nuclear power industry today is in the management and disposal of high-level radioactive waste. Vitrified high-level waste can be stored for about 50 years before ultimate geological disposal. However, in many countries around the world much research effort is being expended in the possibility of partitioning and transmuting radioactive waste, which can reduce it's toxicity by a factor of 100 e.g.[23]. Recently a number of roadmaps for nuclear waste transmutation have been produced e.g. [24]. Although the most frequently discussed methods involve transmutation by bombardment with neutrons from a reactor, there have been other suggested approaches to this problem, for example laser-driven high-brightness gamma generation for photo-transmutation [25].

In this section we report on the use of the VULCAN petawatt laser to drive the photo-transmutation of long-lived $^{129}$I with a half-life of 15.7 million years to $^{128}$I with a half-life of 25 min [26]. A laser-generated gamma ray is absorbed into the $^{129}$I nucleus, which releases a neutron to undergo transmutation to $^{128}$I. This giant dipole resonance ($\gamma$,n) reaction is observed in $^{129}$I and $^{127}$I and the absolute activities of the reaction products $^{128}$I and $^{126}$I are used for the first time to determine an integrated cross-section for $^{129}$I($\gamma$,n)$^{128}$I, from the known $^{127}$I($\gamma$,n)$^{126}$I cross-section Although this reported experiment was carried out on a large laser, the work was simultaneously performed on a compact laser [27] at the University of Jena.

The arrangement on VULCAN was identical to described in the first section but instead of irradiation of targets with protons the relativistic electrons interacted with a 4mm thick Au target and produced high energy gamma rays. These interacted with iodine samples of 85% $^{129}$I and 15% $^{127}$I as shown in Figure 8.

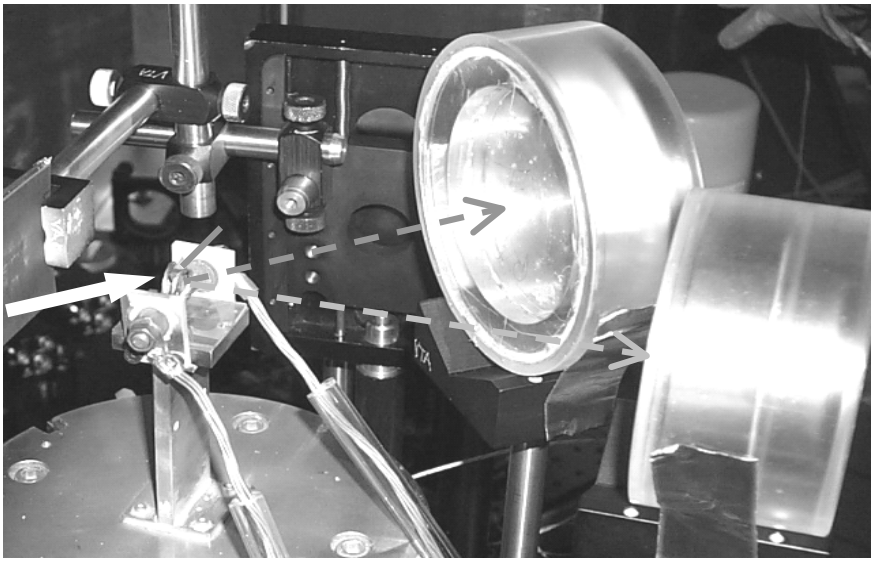

**Fig 8** The laser comes from the left interacting with a Au target to produce gamma rays which irradiated the iodine samples.

The iodine samples were analysed using the germanium detectors before and after laser irradiation of the gold target. The background spectrum of figure 9 was measured for 3 hours and the principal lines observed resulting from the decay include $^{125}$Sb. The background activity from the samples was of the order of $2.4 \times 10^{8}$ Bq.

Figure 9 shows clear peaks at 443.3 keV and 527.1 keV, characteristic of the decay of $^{128}$I. The decay of $^{128}$I was determined by measuring the integrated area of the peaks over successive time intervals. The half-lifes of the 443.3 keV and 527.1 keV peaks were (25.8±1.0) minutes and (25.5±1.5) minutes respectively, which agree well with the literature value of 25.0 minutes. In addition, the ratio of the area of the 443.3 keV and 527.1 keV peaks averaged over all of the measured spectra is 10.9, in good agreement with the literature value of 10.4 From the data we have deduced the total activity of $^{128}$I produced at the time of the laser shot to be 1323 Bq. This corresponds to the production of about $2.9 \times 10^{6}$ nuclei of $^{128}$I for the 360 J laser shot.

The iodine samples contained 15% of the isotope $^{127}$I. Observed weak peaks at 388.6 keV and 666.3 keV in the measured gamma emission spectra are attributed to the decay of $^{126}$I, produced by ($\gamma$,n) reactions on $^{127}$I. A similar analysis performed on those peaks illustrates the production of $1.7 \times 10^{6}$ $^{126}$I nuclei.

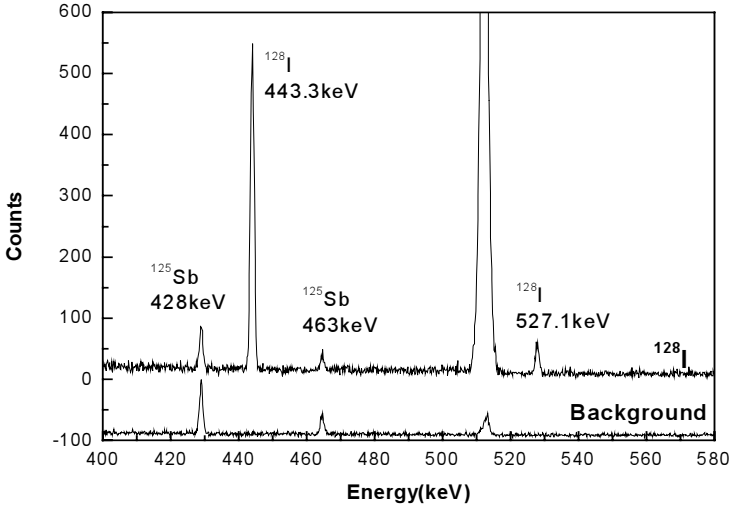


**Fig 9** Gamma emission spectra from one of the iodine samples measured before (background) and after laser irradiation of the gold target. Characteristic emission lines of $^{128}$I at 443.3 keV and 527.1 keV are clearly observed.

Comparison of the numbers of the $^{129}$I(γ,n)$^{128}$I and $^{127}$(γ,n)$^{126}$I reactions induced in the same iodine sample facilitates a ratio of the integrated cross-sections for these reactions to be determined. For a given gamma intensity Φ, the number of nuclei $N_{128}$ of $^{128}$I and $N_{126}$ of $^{126}$I produced are given by: $N_{128}=\sigma_{129}\Phi N_{129}$ and $N_{126}=\sigma_{127}\Phi N_{127}$, where $N_{127}$ (=3.5x10$^{22}$) and $N_{129}$ (=1.8x10$^{23}$) are the initial number of nuclei of $^{127}$I and $^{129}$I respectively in the sample and $\sigma_{129}$ and $\sigma_{127}$ are the cross-sections for the $^{129}$I(γ,n)$^{128}$I and $^{127}$I(γ,n)$^{126}$I reactions respectively. Assuming the Q-value and width of the cross-sections are similar, the ratio of the integrated cross-sections can be written as:

$$\frac{\sigma_{\mathrm{int}}^{129I}}{\sigma_{\mathrm{int}}^{127I}} = \frac{N_{128}}{N_{126}} \cdot \frac{N_{127}}{N_{129}}$$

The integrated cross-section for $^{127}$I(γ,n)$^{126}$I is known, 309 mbarns [19], and the value for the $^{129}$I(γ,n)$^{128}$I reaction was determined using 4 measured spectra to be 97±40 mbarns. This is in good agreement with the theoretical cross-section given in the literature as 110 mbarns [28]. The main uncertainty in the determined integral cross-section resides in the measured gamma-peak areas. It should be emphasized here that at this stage, the laser approach to transmutation is to give an alternative option to the background studies necessary without recourse to accelerators or reactors.

**Acknowledgements** Although there is a single name on this article it would be amiss of me not to mention the talented group of people who work with me and who are largely responsible for the work described. My own group at Strathclyde, Paul McKenna, Lynne Robson, Tom McCanny Seiji Shimizu, Jiamin Yang and

Ravi Singhal at Glasgow . I also acknowledge my colleagues from RAL ad Imperial College and the Laser crew at RAL.

## References


1. Malka V *et al Science,* 2002, **298,** 1596
2. Snavely RA *et al, Phys. Rev. Lett* 2000, **85,** 2945
3. McKenna P *et al, Phys. Rev. Lett* 2003, **91,**
4. Spencer I *et al, Nucl. Instr. and Meth* 2001, **183,** 449-458.
5. Ledingham KWD *et al, J. Phys D: Appl. Phys.* 2004, **37,** 2341-2345.
6. Fritzler S *et al, Applied Physics Letters* 2003, **83,** 3039-3041.
7. Tajima T and Dawson JM, *Phys. Rev. Lett* 1979, **43,** 267
8. Strickland D and Mourou G *Opt. Commun* 1985, **56,** 219-221.
9. Ross IN *et al, Laser Part. Beams* 1999, **17,** 331
10. Dubietis A *et al, Opt. Commun* 1992, **88,** 437
11. Umstadter D; *Physics of Plasmas* 2001, **8,** 1774
12. Spencer I *et al, Rev. Sci. Inst.* 2002, **73,** 3801
13. Wilks SC *et al, Physics of Plasmas* 2001, **8,** 542
14. Allen M *et al, conference proceedings of Field Ignition High Field Physics (Kyoto,Japan)* 2004, p2716
15. Clark EL *et al, Phys. Rev. Lett* 2000, **84,** 670
16. Umstadter D, *J. Phys D: Appl. Phys.* 2003, **36,** R151
17. Zepf M *et al, Physics of Plasmas* 2001, **8,** 2323
18. Hatchett SP *et al, Physics of Plasmas* 2000, **7,** 2076
19. http:IAEAND.IAEA.OR.AT/exfor; *EXFOR nuclear reaction database* 2004,
20. Patel PK, private communication
21. Collier JL and Ross IN, private communication
22. http:www.physik.uni-jena.de/qe/Forschung/F-Englisch/Petawatt/Eng-FP-Petawatt.html; 2004
23 Magill J.*et al Nuclear Energy 2003,* **42,** 263
24 Rubbia C. A European Roadmap for Developing Accelerator Driven Systems for Nuclear Waste Incineration *ENEA Report* (ISBN 88-8286-008-6)
25 Li D, Imasaki K, and Aoki M *J.Nucl.Sci.Technol* 2002, **39,**1247,
26 Ledingham K.W.D. *et al J.Phys.D Appl.Phys* 2003, **36,** L79
27 Magill J *et al Appl Phys B* 2003, **77,** 387.
28 2000 *Handbook on Photonuclear Data for Applications-Cross Sections and Spectra* IAEA-TECDOC-1178.